Novel Combinative Structure of High-Performance Solar Steam Device derived from Areca Nut

Tzu-min Chou[1], Jin-Long Hong[2*]

Department of Materials and Science, National Sun Yat-sen University. Kaohsing 80424, Taiwan, ROC

Abstract**—***A novel combinative structure, consisting of lateral hydrophobic pontoon oAN and central hydrophilic evaporator iAN, was designed for high-performance solar steam device. Both oAM and the iAN were derived from areca nut (AN), through different thermal and surface chemical treatments. With inferior water absorption and evaporation efficiency, the pontoon oAN nevertheless provides footage for the entire device, in contrast, although being efficient in water adsorption and evaporation, iAN requires the supporting oAN to keep its buoyancy. We therefore combined advantages of oAN and iAn to assemble a solar steam device with long-term stability and high solar thermal efficiency of ~82% under 1-sun illumination. The idea using combinative structure as efficient solar steam device can be further extended to other potential systems, therefore, this study provided foundation for future development of novel solar steam devices. importance.*

Keywords**—Solar steam generation, areca nut, pontoon, supporter, combinative structure.**

I. INTRODUCTION

Solar-driven water evaporation[1-8], which utilizes sunlight as a renewable energy source, is a promising approach to provide clean water with minimized environmental impact. Recently, an interfacial evaporation route using non submersible solar steam devices, has been proposed to improve heat localization at the liquid surface, which has successfully achieved high evaporation efficiency[9-17]. In this system, the confined thermal energy selectively heated up the water at the surface, thus minimizing heat loss to bulk water. Moreover, the surface temperature of the absorber is low due to effective evaporation, lowering radiation and convection heat losses at the absorber surface. With this scheme, solar-to-vapour conversion efficiencies can be as high as 90 this aspect, several natural materials, such as plants[18-21], green leaf of Scindapsus aureus[22] and trees[23], had been subjected to different surface treatments to result in interfacial evaporation systems for study.

In general, interfacial system can be classified into direct and indirect contact systems according to the relative position of the solar steam devices to the water surface. Direct contact configuration used self-floating hydrophobic absorbers derived from various materials, such as nanoparticles[24,25] monolithic aerogel and foams[6,26,27], which are all capable of converting light into heat to vaporize the adsorbed water. However, this direct contact system is generally inferior in vaporizing the water, e.g. porous polymer–coding inorganic sheets[25] exhibited a solar thermal conversion efficiency of 63.6% under 1-sun irradiation. Aside from the self-floating means, films consisting of the absorber materials coating on light-weight and hydrophobic scaffolds, such as stainless steel (SS) mesh[3], polypropylene (PP) mesh[28], gauze[29], and carbon fabric[30], were also reported. All these direct contact systems utilized hydrophobic absorbers, which have limited water vaporization routes and are therefore low in photo thermal conversion efficiency.

In contrast, indirect contact system involved a bilayered structure, with the top absorber layer absorbing the solar flux without contacting the bulk water and the bottom supporting layer offering stable support for the top solar steam devices. In general, the bottom layers referred to microporous structure with interconnected channels for efficient water supply, for which carbonized mushroom[31] and basswood[32]were previously used as hydrophilic components containing microporous channels for facile water absorption and vaporization, These carbonized mushroom and basswood exhibited a high conversion efficiency of 78% and 75%, respectively, but their long-term stability needed to be justified as we consider that the water adsorbed by the hydrophilic supporting materials would overload and sink the whole device eventually. The long-term stability problem may be reasonably improved by using hydrophobic supporting system, instead. Previously, polypryrrole was used as the absorbent layer[30]on top of the supporting polypropylene (PP) membrane. This served as insulating layer minimizing the heat loss of the device to the bulk water, however, the reverse effect of the hydrophobic PP in preventing the water adsorption should just the conversion efficiency (58%) of the device.

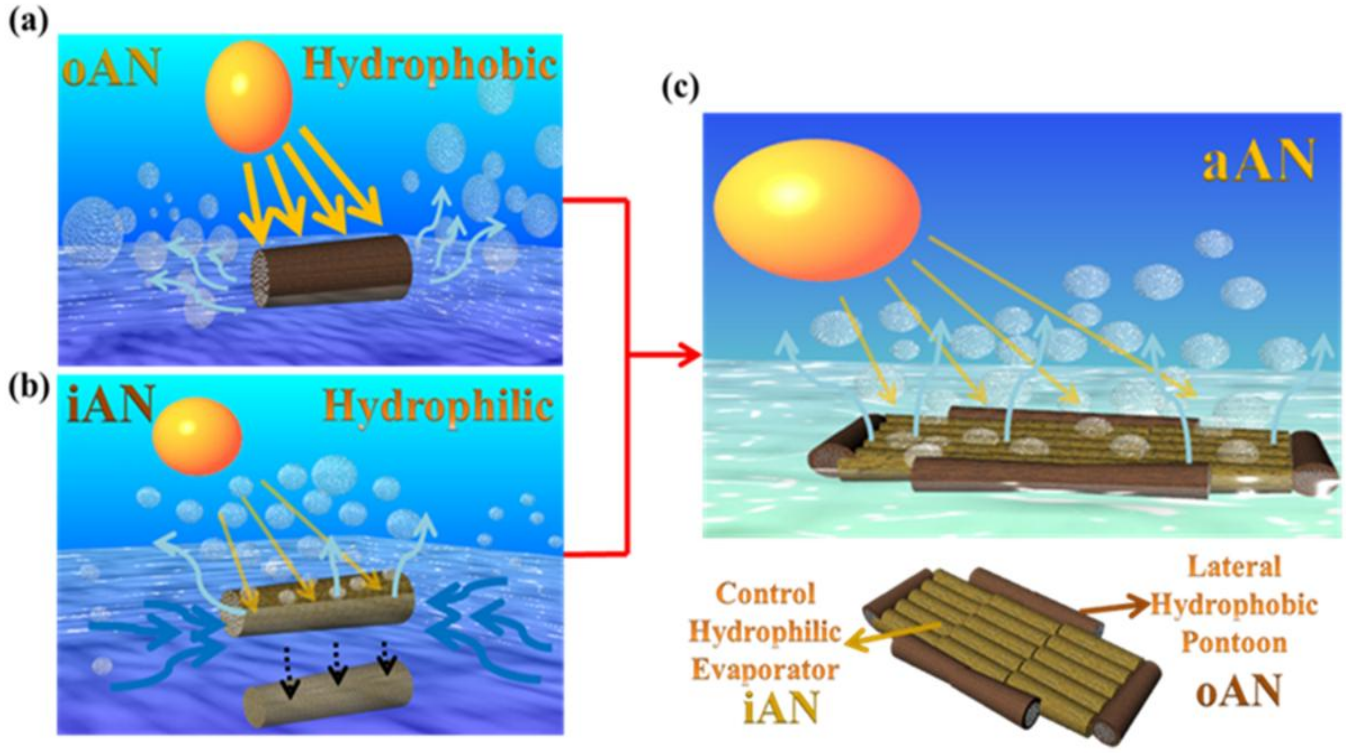

SCHEME 1: Illustrations of shortcomings of hydrophobic oAN (upper left) and iAN (lower left), and the combinative solar steam device of aAN (right) containing the lateral oAN pontoons and central iAN evaporator.

Rather than a bilayered structure mentioned above, this paper imparts new idea of using lateral pontoon (upper left, Scheme 1) as efficient supporting component to lift the central evaporator (lower left) over the water surface for a long time. Through surface thermal and chemical modifications of the natural areca nut (AN), both hydrophobic oAN pontoon and hydrophilic iAN evaporator can be successfully prepared and combined to fabricate a solar steam device of aAN (right) with separate supporting and evaporating components. Supposedly, water-resistant oAN is a perfect pontoon capable of floating whole device over the water surface but the vapors produced by sun heat would bypass the oAN, which prohibits the potential of using oAN as water evaporator, due to the water-repellency of the hydrophobic oAN. On the other hand, hydrophilic iAN enables the efficient water absorption and vaporization but along the process, the infiltrated water inside iAN would eventually overload and sink the whole device into the cold underwater, at which place iAN is unable to function properly as water evaporator. Nevertheless, shortcomings of oAN and iAN can be smartly avoided by assembling both components into one single aAN device, which contains both the lateral oANs and the central iAN as the supporting and steam-generation parts (lower left), respectively.

II. RESULTS AND DISCUSSION

Taking advantage of the unique structure of the integrated aAN device (Scheme 2), functions of solar steam-generation, water pumping and evaporation as well as supporting pontoon are decoupled into two components, with central hydrophilic iAN for water pumping and evaporation and the lateral hydrophobic carbon black nanoparticles CM-coated oAN for lifting the whole device over water surface. The central iAN and the lateral oAN prepared from different thermal and chemical surface treatment procedures were then glued together to result in the aAN-based solar steam device capable of standing over water surface for long enough time (> 1 month). To prepare iAN and oAN, we needed to peel off the green shell of AN and cut it into two pieces. The enriched vascular bundle structure (magnified part of the upper leftmost) of the cut piece is beneficial for water adsorption and transport. The cut pieces were then dried under vacuum for 24 hr to obtain the dried AN for different treatments to result in iAN and oAN, respectively.

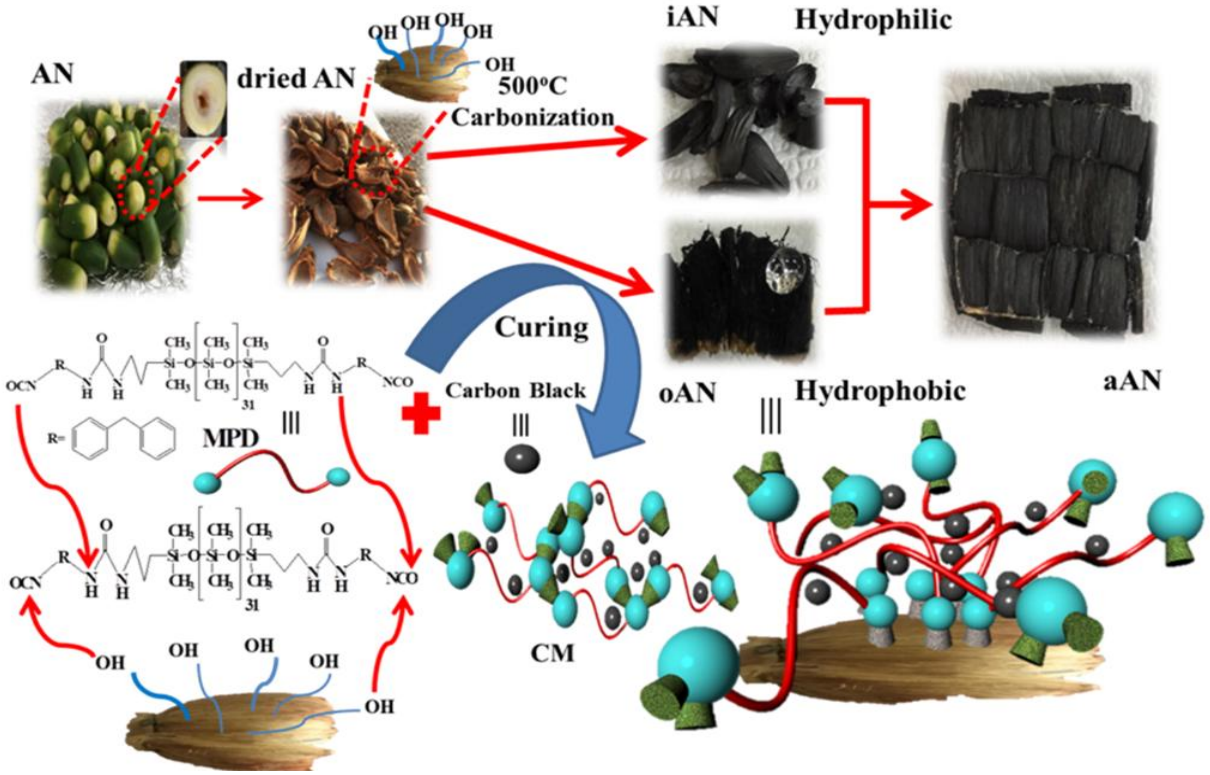

SCHEME 2: Preparation process of aAN-based solar steam device.

Direct carbonization of the dried AN in a horizontal tubular reactor at 500°C for 2 hr provided hydrophilic iAN (Scheme 2) for use. In contrast, preparation of oAN required delicate chemical modification using a methylene diphenyl diisocyanate (MDI)-terminated poly (dimethyl siloxane) (MPD, cf. Experimental section for synthesis) as the multi-functional reagent, which enabled the facile crosslinking reactions between isocyanate groups of MPD and phenolic functions over the surface of the dried AN and also, served as excellent dispersant of carbon black (CB). End-capping of an amine-terminated poly (dimethyl siloxane) (PD) with hexamethyl diisocyanate (HDI) afforded MPD with urea linkages and isocycante functional groups at the ends. Previous study[33] in our lab already verified the facile self-reaction of MPD that its urea linkages can attack its isocyanate terminals (lower) to result in hydrophobic crosslinking network. In the presence of dried AN, additional inter-reaction between isocyanate terminals of MPD and the surface phenolic OH functions of AN acted to reinforce the interfacial adhesion between the resulting crosslinked network and dried AN. Moreover, the MPD can be an excellent dispersant for CB, which can mix with equal weight of CB in tetrahydrofuran (THF) solvent to result in homogenous solution with long term stability. The hydrogen bond interactions between the urea NH and urea C=O of MPD and the COOH of CB are responsible for the homogeneous dispersion of CB by MPD. The homogenous THF solution was then applied over the surfaces of the dried ANs before being heated at 120 °C for 3 hr to result in homogenous CB-included CM composite. Large amounts of CB in CM composite should be gripped firmly by the crosslinked network since we see no sign of CB leakage after the whole aAN component had been placed on water for a long time (>1 month).

Scanning electron microscopy (SEM) images of iAN (Fig. 1(a)-(b)) revealed its unique structure beneficial for the water adsorption, transport and vaporization. SEM morphology of iAN (Fig. 1(a) is similar with AN (Fig. 1(e)), which suggests that the enriched water paths in the pristine survive after high-temperature carbonization at 500°C. The enriched water paths of iAN were ensured by the abundant macro (red circle, Fig. 1(b)) and micro (blue circle) pores in the xy plane, as well as the macro (blue circle, Fig.1(c)) and micro (red circle) cylindrical channels in the yz plane. All the pores and channels with few to several micrometers in sizes formed a continuous 3D porous network, which provides versatile routes for the water adsorption and transport. Under the assistance of capillary force and additional driving force induced by water evaporation, water transported fluently from the bottom of bulk water to the top surface of iAN. In addition, the peeling of surface layer during preparation step left a plethora of broken channels (Fig. 1(d)) on the surface of iAN, which are open to the air and under sunlight illumination, the open channels provide facile vaporization paths to the air.

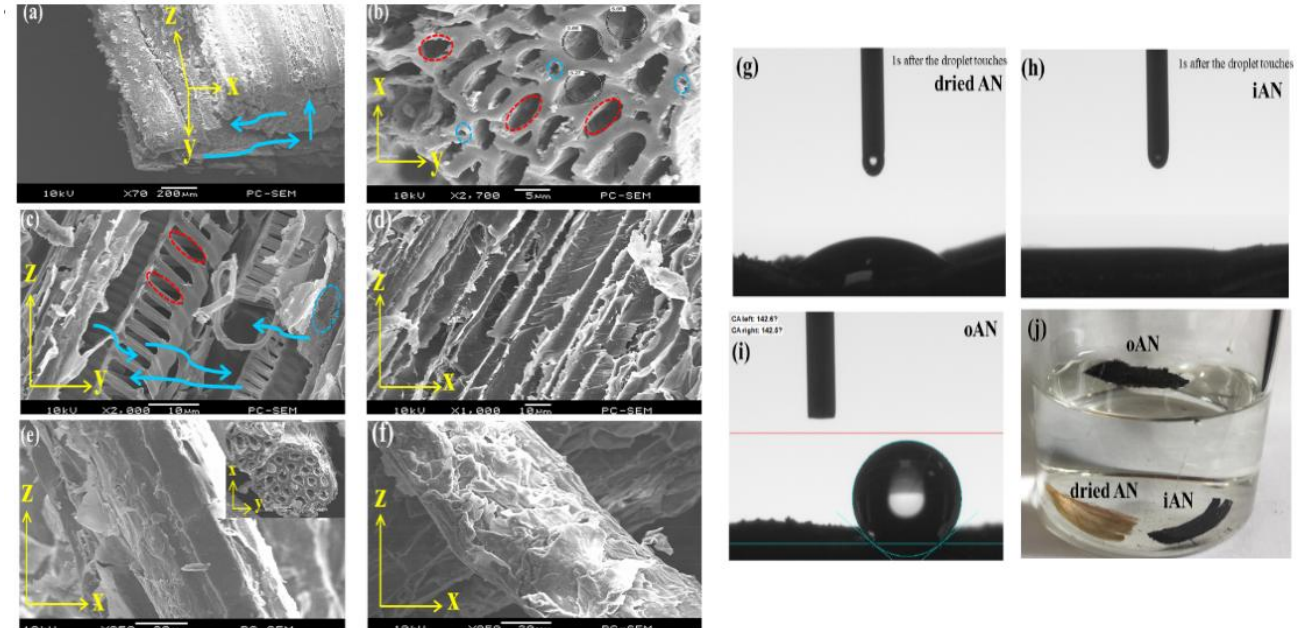

FIG. 1. SEM images of (a) iAN with the x, y, and z directions, (b) iAN with the macro (red circle) and micro (blue circle) pores in spherical shape, (c) iAN with the macro (blue circle) and micro (red circle) channels in cylindrical shape, (d) surface view of iAN with the broken vessels, (e) dried AN and (i) oAN with the rough surfaces. Absorptions of water droplets by the surfaces of (g) dried AN and (h) iAN, and (i) AN and (j) optical images of the floating oAN and the sunken An and iAN.

Moreover, SEM can identify the morphological difference between dried AN (Fig. 1(e)) and oAN (Fig. 1(f)). Except the broken channels, surface of dried AN is relatively smooth compared to the rough, wrinkled surface of oAN. The rough surface of oAN is full of the CB-included CM composite, which is hydrophobic layer with repellence to the incoming water. This rough, wrinkled surface of oAN is of great importance in view that such morphology dramatically raised the surface roughness to provide a composite interface in which air became trapped within the grooves under water, therefore inducing hydrophobicity with phenolic OH groups and the enriched porous structure, dried AN can absorb water readily. After carbonization, the enriched pores and channels of iAN provided the fluent water absorption and transport paths and therefore, the hydrophilicity of the sample. Surface wetting is another important parameter, which influences interfacial solar membrane performance. The round water droplet deposited on the surface of the dried AN was still elliptical in shape within 1 s (Fig. 1(g)), in contrast, the round water droplet was completely absorbed by the hydrophilic iAN (Fig. 1(h)) within the same 1 s period. A hydrophobic surface with excellent water droplet roll-off is the desired property of oAN, which depends not only on the chemical nature on the hierarchical structure of the surface. Due to the nanoscale roughness and the hydrophobic nature of the CM coating, the modified oAN is hydrophobic in nature and the water droplet, dropped on the surface of oAN, immediately rolled off (Fig.1(i)) and yet, kept the spherical shape with a high contact angle ($> 140^{o}$). Even when pressed into the water, the black hydrophobic oAN can spontaneously float again (Fig.1(j)) because of the air "cushion" of the hydrophobic surface. In comparison, the dried AN and the carbonized iAN would sink into the bottom of the beaker as time goes by. Because the hydrophobic oAN can float on the air-water interface for a long time, it should serve well as pontoon to float the aAN device.

We chose CB as the light-absorbing material, because CB is a natural light absorber with a rich source of raw materials, together with very mature and low-cost industrial production. The incorporation of crosslinked network with CB resulted in stable light absorber of CM, which can be seen from comparing the optical properties of iAN with other light-absorbing materials (Fig. 2(a)), such as CM-coated wood and paper. The absorbance (A), reflectance (R) and transmittance (T) in the wavelength range from 190 nm to 2250 nm can be easily detected and analyzed with the simple relationship of $A = 1 – R – T$. As shown in Fig. 2(b) and (c), iAN is low in reflectance (less than 5% in the visible light region and less than 10% in the whole measurement region) and exhibits a near-zero transmittance. Accordingly, the absorbance of iAN (> 92 %, Fig. 2(d)) is superior to CM-coated wood and paper throughout the whole measurement region, which provides foundation for using iAN as the water evaporator in this study.

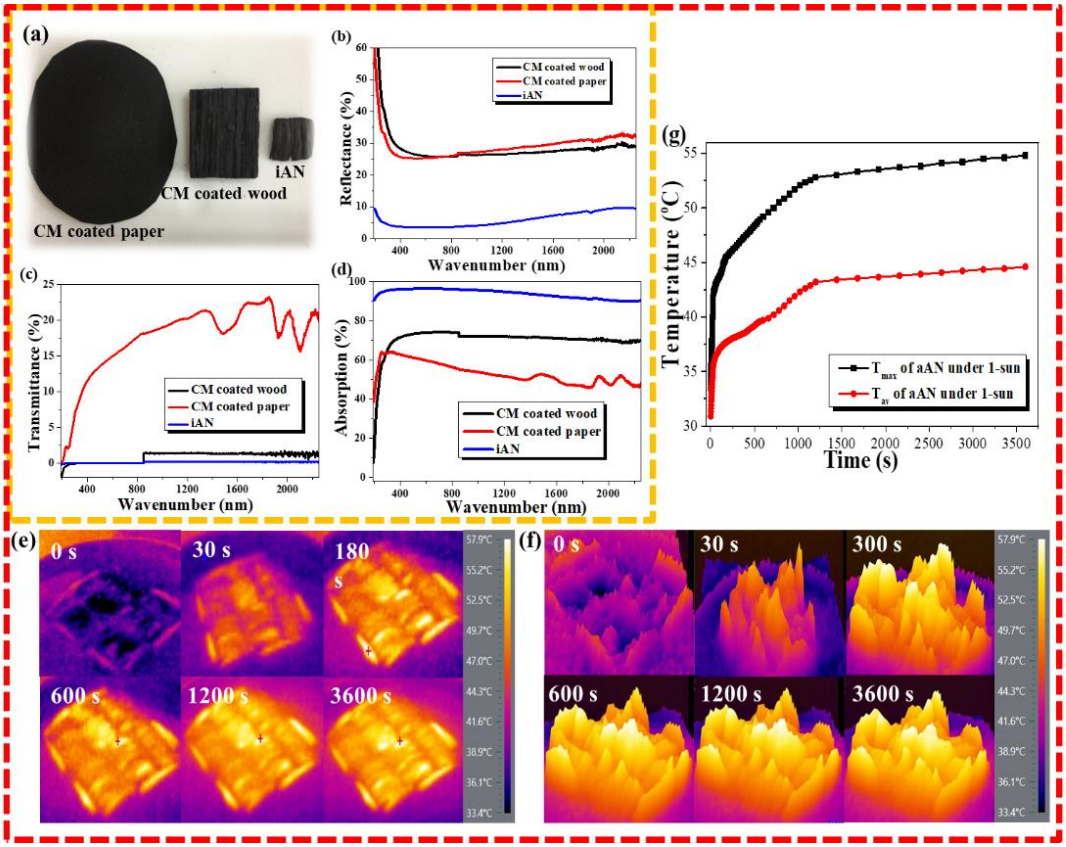

FIG. 2. (a) The appearance of oAN and the CM-coated wood and paper, and the UV-Vis spectra to trace the (b) reflectance, (c) transmittance and (d) absorbance in the wavelength range from 190 nm to 2250 nm, (e) Infrared photos of the aAN surfaces, (f) 3D display of infrared photos of the aAN surfaces, in order from left to right, correspond to t = 0, 30, 180, 600, 1200, and 3600 s after illumination and (g) maximum and average temperatures of the surfaces of aAN as a function of time.

To evaluate the enhanced water vaporization of the free-floating aAN device, infrared thermal images (Fig. 2(e)) along with the 3D display (Fig. 2(f)) under 1-sun intensity were captured and the temperature profiles of aAN and the surrounding water were detected and analyzed. Temperature of aAN was relatively low (34^{o}C) initially, indicating strong intrinsic evaporation as expected. The maximum (T_{max}) and average (T_{av}) temperatures plotted in Fig. 2(g) give clear view on temperature variation as a function of illumination time that both T_{max} and T_{av} rose rapidly once the illuminating light was turned on. Within 20 min of light irradiation, both T_{max} and T_{av} reached steady values and after 1 hr of illumination, T_{max} and T_{av} both reached 54 °C and 44^{o}C, respectively, which are high due to the high absorbance (> 92%) of the iAN evaporator.

We then compared the evaporation rates and energy conversion efficiencies of the integrated aAN with CM-coated paper and wood by accurate examination of the corresponding weight changes (Fig. 3(a)) of all samples under 1-sun illumination. The aAN exhibited the largest mass changes among all samples, including pure water, oAN, iAN and CM-coated wood and paper. The evaporation rates here were calculated from the slope of the resolved curves, which gave relative evaporation rates of all samples under illumination. Here, because of the larger evaporating areas endowed by high fraction of pores and channels, the aAN exhibited a high evaporation rate of 1.31 kg m^{-2} h^{-1}, which is comparatively higher than those of CM-coated paper (0.83 kg m^{-2} h^{-1}) and wood (0.38 kg m^{-2} h^{-1}) as well as oAN (0.18 kg m^{-2} h^{-1}) and iAN (0.54 kg m^{-2} h^{-1}). The hydrophobic CM coating tends to repel water to result in inferior water evaporation rates of the CM-coated paper, wood and oAN. The inferior evaporation rate of oAN and iAN indicates that both components are essential parts for aAN and cannot serve alone as efficient solar steam device. As the concepts illustrated in Scheme 1, the limited water absorption of the hydrophobic oAN and the inferior water evaporation of the submersible iAN are responsible for the low efficiencies of iAN and oAN, respectively. The energy conversion efficiency (η) is defined $\eta = \dot{m}h_{lv}/P_{in}$, where $\dot{m}$ is the mass flux of steam, denotes the liquid–vapor phase change enthalpy, and P_{in} is the received power density of light illumination. In our instance, the efficiency of aAN was calculated to be 82% (Fig. 3(b)), which is higher than those of oAN (11%), iAN (34%), CM-coated paper (52%) and wood (24%).

The real durability of aAN in seawater needed to be considered for practical application and in this aspect, simulated sea water (a 3.5 wt% NaCl aqueous solution) under a simulated solar light intensity of 1-sun was applied and the desalination results were summarized in Fig. 3(e)-(f). Over the seawater for 2 hr, the wetted aAN was weighted to determine the weight change and dried in oven before next cyclization measurement. It is found that the performance is maintained for at least 5 cycles, with each cycle being over 2 hr. The resolved weight changes (Fig. 3(c)) over 5 cycles are almost the same and the calculated efficiency changes followed the same pattern that the initial efficiency curve versus time (Fig. 3(d) increased rapidly before becoming flatten, similar with the efficiency curve of sea water. According to the result, the efficiency retentions (Fig. 3(e)) over 5 cycles are almost the same, all with the resolved straight line paralleling to the X-axis, which points out that the solar steam device of aAN with a combinative structure is excellent in durability. It is curious to know the salt deposition situation, which can be evaluated from the SEM images of the samples after 5 cycles of 1-sun illumination, on the hydrophobic oAN (left, Fig. 3(f)) as well as the hydrophilic iAN (right). For oAN, few NaCl particles (yellow arrows) were deposited on the external surfaces, which suggested that adsorption of the saltwater was blocked by the hydrophobic surface of oAN. In contrast, the large amounts of salts were deposited over the outside and inside of the pores present in iAN sample, which clearly demonstrated the capability of iAN in adsorbing, transporting and vaporizing seawater. The NaCl salts in saltwater resulted in an evaporation efficiency (76%) slightly lower than that (82%) from the pure water, nevertheless, the resolve value of 76% is still higher than most of the reported data. Conductivity from LCR meter can be used to measure NaCl concentration in the saltwater before and after desalination. The concentration of sodium ion collected from the water in the condensation chamber was significantly decreased by at least four orders of magnitude after desalination, which was far below the salinity levels defined by World Health Organization (WHO), i.e. 1000 mg L^{-1} and the US Environmental Protection Agency, i.e. L^{-1}, respectively. The successful solar desalination process of NaCl solution (3.5 wt%) further proves that our aAN exhibits good salt resistant property.

III. CONCLUSION

In summary, we have introduced a novel solar steam device aAN, with lateral hydrophobic oAn as supporting pontoon and central hydrophilic iAN as evaporator, for highly efficient solar steam device. With the hydrophobic CB-coated CM outer layer, oAN acted as efficient supporting material, in contrast, owing to the natural vessel structure and hydrophilicity, the iAN formed an ideal water adsorption, transport and vaporization system for solar steam device. In our instance, the efficiency of aAN was calculated to be 82%, which is higher than those of oAN (11%), iAN (34%), CM-coated paper (52%) and wood (24%). Although the evaporation of seawater by aAN is lower than that of pure water system, the desalination process still maintained a high conversion efficiency of 76% and showed a high value of 72% after 5 experiment cycles. Importantly, we had demonstrated that AN, a low-cost material ($1.1 per kg), which can be easily obscured in the street corners of Asian cities, can be used to derive efficient solar steam device, through ingenious design idea using pontoon as separate supporting component. The idea of using pontoon as separate component of an efficient device can be extended to other existing or potential hydrophilic light absorbers, e.g. paper and wood.

IV. EXPERIMENTAL SECTION

4.1 Materials

Good-quality AN was purchased from a betel nut stand in Kaohsiung city, Taiwan. Amino-terminated poly(dimethyl siloxane) (PD, M_w~ 2,500 g/mol), MDI and CB were all purchased from Sigma-Aldrich. Tetrahydrofuran (THF) was refluxed with benzophenone and sodium for 2 days in prior to distillation for use.

4.1.1 Preparation of hydrophilic carbonized areca nut (iAN)

Before carbonization, AN was dried under sun light at least 24 hr after thorough washing to remove any greasy or dust materials. The sun-dried AN was then heated in an oven at 120°C for 24 hr to remove moisture. Carbonization was carried out in a horizontal tubular reactor at 500^{o}C for 2hr under nitrogen flow. The heating rate and nitrogen flow rate were 5°C/min and 200 mL/min, respectively. The sample was cooled down to room temperature under nitrogen atmosphere and was labeled as iAN (yield = 78%).

4.1.2 Preparations of MPD

MPD was required to be prepared first by the reported procedures[33]. Before reaction, PD needed to be dried under vacuum at 80^{o}C for 1 hr. Then, into an argon-blanketed, vigorously-stirred solution of PD (0.5 g, 0.1 mmol) in THF (10 mL), solution of MDI (55 mg, 0.2 mmol) in THF (5 mL) was added dropwise. The resultant mixture was then heated at 60^{o}C for 5 hr under

argon atmosphere. Then the reaction mixtures were subjected to vacuum distillation at 70^{o}C to remove most of the residual THF to obtain the desired MPD.

4.1.3 Preparation of hydrophobic MPD/CB (CM)-coated oAN

The unmodified AN was dried under sunlight for at least 24 hr after thorough washing to remove any greasy or dust materials. The sun-dried AN was then heated in an oven at 120°C for 24 hr to remove moisture. The dried AN was then immersed into a solution of MPD and CB in THF and the whole solution mixtures were stirred for another 2 hr for maximizing the absorption of MPD and CB. The MPD can be an excellent dispersant for CB, which can mix with equal weight of CB in tetrahydrofuran (THF) solvent to result in homogenous solution with long term stability. Then, the MPD/CB (CM) - coated AN was heated to cure at 120^{o}C for 3 hr to obtain the desired oAN.

4.2 Characterization

Scanning electron microscope (SEM) images were recorded using a Jeol JSM-6700F microscope operated at 10 kV. A Krüss GH-100 goniometer interfaced to image-capture software was used to measure the static WCA. For the contact angle of water droplet (5 uL) over surface of AN, iAN and oAN were measured using an FDSA MagicDroplet-100; each reported contact angle represents the average of six measurements. The simulated solar irradiation was provided by a MFS-PV BASIC (Hong-Ming Technology Co., Ltd.). Solar and the light intensity was adjusted to 1000 W m^{-2}. The UV-v is absorption, transmittance and reflectance spectra were recorded with a JASCO V-770 spectrophotometer. IR images of infrared photos were taken by IR Thermographic Camera (Sonel KT-80). The 3D display of infrared photos is draw using the Sonel ThermoAnalyze2 software. The electric properties were determined at room temperature by an LCR meter (Tonghui TH2829) at 1 kHz with taking five points for each data to average. The measurement distance of the two resistance measurers is fixed at 1 cm. The 1H NMR spectra were recorded by a Varian Unity VXR-500 MHz instrument. FTIR spectra were recorded from a Bruker Tensor 27 FTIR spectrophotometer; 32 scans were collected at a spectral resolution of 1cm^{-1}. The solid powders were homogeneously blended with KBr before pressed to make pellets for measurement.

ACKNOWLEDGEMENTS

This work is supported by the Ministry of Science and Technology (MOST), Republic of China (ROC), under the contractMOST107-2221-E-110 -015.

REFERENCE

[1] M. Gao, L. Zhu, C. K. Peha and G. W. Ho, Solar absorber material and system designs for photothermal water vaporization towards clean water and energy production. Energy Environ.Sci.2019, pp. 841–864

[2] J. Huang, Y. He, L. Wang, Y. Huang and B. Jiang, Bifunctional Au@ TiO_2 core–shell nanoparticle films for clean water generation by photocatalysis and solar evaporation. Energy Convers. Manag.2017, 132, 452-459.

[3] J. Lou, Y. Liu, Z. Wang, D. Zhao, C. Song, J. Wu, N.Dasgupta, W. Zhang, D. Zhang, P. Tao, W. Shang and T.Deng, Bioinspired multifunctional paper-based rGO composites for solar-driven clean water generation. ACS Appl. Mater. Interfaces2016, 8, 14628-14636.

[4] Y. Liu, J. Chen, D. Guo, M. Cao and L. Jiang, Floatable, self-cleaning, and carbon-black-based superhydrophobic gauze for the solar evaporation enhancement at the air–water interface. ACS Appl. Mater. Interfaces, 2015, 7, 13645-13652.

[5] P. Zhang, J. Li, L. Lv, Y. Zhao and L. Qu, Vertically aligned graphene sheets membrane for highly efficient solar thermal generation of clean water. ACS Nano 2017,11, 5087-5093.

[6] L. Zhu, C. F. Tan, M. Gao and G. W. Ho, Design of a Metal Oxide–organic framework (MoOF) foam microreactor: solar-induced direct pollutant degradation and hydrogen generation. Adv. Mater.2015, 27, 7713-7719.

[7] L. Zhu, M. Gao, C. K. N. Peh, X. Wang and G. W. Ho, Self-contained monolithic carbon sponges for solar-driven interfacial water evaporation distillation and electricity generation. Adv. Energy Mater. 2018, 8, 1702149.

[8] L. Zhu, M. Gao, C. K. N. Peh and G. W. Ho, Solar-driven photothermal nanostructured materials designs and prerequisites for evaporation and catalysis applications. Mater. Horizons 2018, 5, 323-343.

[9] P. Tao, G. Ni, C. Song, W. Shang, J.Wu, J. Zhu, G. Chen and T. Deng, Solar-driven interfacial evaporation. Nature Energy 2018, 3, 1031–1041.

[10] Z. Wang, Y. Liu, P. Tao, Q. Shen, N. Yi, F. Zhang, Q. Liu, C. Song, D. Zhang, W. Shang, and T. Deng,Bio-inspired evaporation through plasmonic film of nanoparticles at the air–water interface. Small. **2014** Aug 27; 10(16):3234-9.

[11] H.Ghasemi, G. Ni, A. Marie Marconnet, J. Loomis, S.Yerci, N.Miljkovic and G. Chen, Solar steam generation by heat localization. Nature Commun.2014, 5, 4449.

[12] Zhang P, Li J, Lv L, Zhao Y and Qu L,Vertically aligned graphene sheets membrane for highly efficient solar thermal generation of clean water. ACS Nano 2017, 11, 5087-5093.

[13] P.Yang, K. Liu, Q. Chen, J. Li, J.Duan, G.Xue,Z. Xu, W.Xie and J. Zhou, Solar-driven simultaneous steam production and electricity generation from salinity. Energy Environ. Sci. 2017, 10, 1923-1927.

[14] L. Zhou, Y. Tan, B. Zhu,P. Zhang,J. Xu, Q. Gan,Z. Yu and J. Zhu,Self-assembly of highly efficient, broadband plasmonic absorbers for solar steam generation. Sci. Adv. **2016**, 2, e1501227.

[15] L. Zhou, Y. Tan, J. Wang, W. Xu, Y. Yuan, W. Cai, S. Zhu and J. Zhu.3D self-assembly of aluminium nanoparticles for plasmon-enhanced solar desalination Nat. Photonics.2016, 10, 393-398.

[16] J. Wang, Y. Li, L. Deng, N. Wei, Y. Weng, S. Dong, D. Qi, J.Qiu, X. Chen and T. Wu,High-performance photothermal conversion of narrow-bandgap Ti_2O_3nanoparticles. Adv. Mater. 2017, 29, 1603730.

[17] H. Ren, M. Tang, B. Guan, K. Wang, J. Yang, F. Wang, M.Wang, J. Shan, Z. Chen, D. Wei, H. Peng and Z. Liu,Hierarchical graphene foam for efficient omnidirectional solar–thermal energy conversion. Adv.Mater. 2017, 29, 1702590.

[18] J. Song, C. Chen, C. Wang, Y. Kuang, Y. Li, F. Jiang, Y. Li, E. Hitz,Y. Zhang, B. Liu, A. Gong, H. Bian, J. Zhu, J. Zhang, J. Li and L. Hu,High-performance solar steam device with layered channels: artificial tree with a reversed design. ACS Appl. Mater. Interfaces 2017, 9, 23520.

[19] C. Jia, T. Li, C. Chen, J. Dai, I. M. Kierzewski, J. Song, Y. Li, C. Yang,C. Wang and L. Hu,Scalable, anisotropic transparent paper directly from wood for light management in solar cells. Nano Energy 2017, 36, 366.

[20] C. Chen, Y. Zhang, Y. Li, Y. Kuang, J. Song, W. Luo, Y. Wang, Y. Yao,G. Pastel, J. Xie, L. Hu, Rich mesostructures derived from natural woods for solar steam generation. Adv. Energy Mater. 2017, 7, 1700595.

[21] K.-K. Liu, Q. Jiang, S. Tadepalli, R. Raliya, P. Biswas, R. R. Naik, S. Singamaneni, Wood–graphene oxide composite for highly efficient solar steam generation and desalination. ACS Appl. Mater. Interfaces 2017, 9, 7675−7681.

[22] S. Zhuang, L. Zhou, W. Xu, N. Xu, X. Hu, X. Li,G.Lv, Q. Zheng, S. Zhu, Z. Wang, and J. Zhu, Tuning transpiration by interfacial solar absorber-leaf engineering. Adv. Sci.2018, 5, 1700497.

[23] C. Chen, Y. Zhang, Y. Li, J. Dai, J. Song, Y. Yao, Y. Gong,I. Kierzewski, J. Xie and L. Hu,All-wood, low tortuosity, aqueous, biodegradable supercapacitors with ultra-high capacitance. Energy Environ. Sci. 2017, 10, 538-545.

[24] Z. Wang, Y. Liu, P. Tao, Q. Shen, N. Yi, F. Zhang, Q. Liu, C.Song, D. Zhang,W. Shang and T. Deng, Bio-inspired evaporation through plasmonic film of nanoparticles at the air–water interface. Small 2014,10,3234-3239.

[25] Z. Hua, B. Li, L. Li, X. Yin, K. Chen and W. Wang, Designing a novel photothermal material of hierarchical microstructured copper phosphate for solar evaporation enhancement. J. Phys.Chem. C 2017, 121, 60-69.

[26] X. Hu, W. Xu, L. Zhou, Y. Tan, Y. Wang, S. Zhu and J. Zhu, Tailoring graphene oxide-based aerogels for efficient solar steam generation under one sun. Adv. Mater. 2017, 29, 1604031.

[27] Y. Fu, G. Wang, T. Mei, J. Li, J. Wang and X. Wang, Y. Fu, G. Wang, T. Mei, J. Li, J. Wang and X. Wang, Accessible graphene aerogel for efficiently harvesting solar energy. ACSSustain, Chem. Eng. 2017, 5, 4665-4671.

[28] M. Ye, J. Jia, Z. Wu, C. Qian, R. Chen, P. G. O'Brien, W.Sun, Y. Dong and G. A. Ozin,Synthesis of black TiOx nano particles by Mg reduction of TiO_2nanocrystals and their application for solar water evaporation. Adv. Energy Mat. 2017,7, 1601811.

[29] M. W. Higgins, A. R. Shakeel Rahmaan, R. R. Devarapalli,M. V. Shelke and N. Jha, Carbon fabric based solar steam generation for waste water treatment. Sol. Energy, **2018**, 159, 800-810.

[30] X. Huang, Y.-H. Yu, O. de Llergo, S. M. Marquez and Z.Facile, Cheng, Facile polypyrrole thin film coating on polypropylene membrane for efficient solar-driven interfacial water evaporation. RSC Adv. 2017, 7, 9495-9499.

[31] N. Xu, X. Hu, W. Xu, X. Li, L. Zhou, Mushrooms as efficient solar steam-generation devices. Adv. Mater. **2017**, 29, 1606762.

[32] Y.Kuang, C. Chen, S. He, E. M. Hitz, Y, Wang, W. Gan, R. Mi, and L. Hu, A High-performance self-regenerating solar evaporator for continuous water desalination. Adv. Mater. 2019, 1900498

[33] C.H.Chung, W.C. Liu and J.L. Hong, Superhydrophobic melamine sponge modified by cross-linked urea network as recyclable oil absorbent materials. Ind. Eng. Chem. Res. 2018, 57, 25, 8449-8459.